Effective Toughness of Heterogeneous Materials with Rate-Dependent Fracture Energy

Gabriele Albertini, Mathias Lebihain, François Hild, Laurent Ponson, David S Kammer

Effective toughness of heterogeneous materials with rate-dependent fracture energy

Gabriele Albertini,[1,2] Mathias Lebihain,[3,4] François Hild,[5] Laurent Ponson,[4] and David S. Kammer[1,*]

[1] *Institute for Building Materials, ETH Zurich, Switzerland*
[2] *School of Civil and Environmental Engineering, Cornell University, Ithaca NY, 14853, USA*
[3] *Laboratoire Navier, ENPC/CNRS/IFSTTAR, France*
[4] *Institut Jean le Rond d'Alembert, Sorbonne Université/CNRS, France*
[5] *Laboratoire de Mécanique et Technologie (LMT), ENS Paris-Saclay/CNRS, France*

(Dated: June 9, 2021)

We investigate dynamic fracture of heterogeneous materials experimentally by measuring displacement fields as a rupture propagates through a periodic array of obstacles of controlled fracture energy. Our measurements demonstrate the applicability of the classical equation of motion of cracks at a discontinuity of fracture energy: the crack speed jumps at the entrance and exit of an obstacle, as predicted by the crack-tip energy balance within the brittle fracture framework. The speed jump amplitude is governed by the fracture energy contrast and by the combination of rate-dependency of fracture energy and inertia of the medium, which allows the crack to cross a fracture energy discontinuity at constant energy release rate. This discontinuous dynamics and the rate-dependence cause higher effective toughness, which governs the coarse-grained behavior of these cracks.

Many biological materials, such as bone, nacre and tooth, have intricate microstructures which are responsible for remarkable macroscopic mechanical properties [1, 2]. Carefully designed microstructures combined with advances in micro-fabrication techniques allow for the development of new materials with unprecedented properties [3–8]. Understanding how to harness small-scale heterogeneities is, however, necessary to achieve the desired macroscopic properties. For fracture properties, recent research focused either on disordered microstructures, where randomly located obstacles distort the crack front and cause toughening by collective pinning [9–12], or on elastic heterogeneities, where compliant inclusions provide toughening by effectively reducing the energy flow into the crack tip [13, 14]. However, a complete and fundamental theory for effective material resistance against fracture remains missing, and experimental observations, which are key for establishing such theoretical knowledge, are scarce.

Theoretical fracture mechanics, based on the seminal work of Griffith [15, 16] states that a crack will propagate as soon as the released elastic energy per unit increment of crack length $G^{\mathrm{S}} = -\partial_l \Omega$, where Ω is the elastic energy in the medium and l the crack length, balances the local fracture energy Γ (*i.e.*, the energy necessary for creating two unit surfaces). During dynamic crack propagation, the energy balance further includes inertia of the surrounding medium and possible rate-dependence of the fracture energy $\Gamma(v)$, where $v = \dot{l}$ is the crack speed. Using Linear Elastic Fracture Mechanics (LEFM) theory [17], one can derive the equation of motion of a crack from this energy balance by assuming steady state crack propagation in an unbounded homogeneous domain. Under these circumstances the crack has no inertia (there is no term involving $\ddot{l}$ in the equation of motion) and its speed adapts abruptly to accommodate changes in fracture energy. However, it remains unclear if these idealized conditions are valid at discontinuities within heterogeneous materials and how they affect the coarse-grained behavior of the crack during dynamic propagation.

In this Letter, we analyze these questions in depth through the experimental investigation of crack propagation in heterogeneous media with fracture energy discontinuities. Usually, fracture mechanics experiments are based on global measurements, thus, only capture averaged quantities. In contrast, our experimental setup and simplified 2D geometry with periodic heterogeneities allows local measurements of the near-crack-tip fields, which support the uncovering of fundamental mechanisms. While the elastic energy release rate is constant as the crack faces a fracture energy discontinuity, the speed at which the crack propagates is observed to vary discontinuously. We study the amplitude of the speed jumps as the crack crosses the interface between regions of different fracture energy and show that it stems from the combination of rate-dependency of fracture energy and inertia of the medium. Rate-dependent effects result from the non-equilibrium nature of fracture problems and are prevailing in materials. Thus, rate-dependent fracture energy applies to a wide range of materials and has been observed, for instance, on rock [18, 19], glassy polymers [20–26] and metals [27]. The discontinuous dynamics and the rate-dependent effects significantly affect the effective toughness of heterogeneous materials, as we will show with our experimental observations.

Our experimental setup (see FIG. 1a) consists of a tapered double cantilever beam, made of multi-material 3D-printed polymers (Stratasys Objet260 Connex3), a high-speed camera (Phantom v2511) and an electromechanical testing machine (Shimadzu AG-X Plus). The matrix material is VeroClear with static fracture energy $\Gamma_0^M \approx 80$ J/m^2 and Young's modulus $E^M \approx 2.8 \pm 0.2$ GPa. The obstacle material is VeroWhite-DurusWhite ($\Gamma_0^O \approx 106$ J/m^2, $E^O \approx 1.9 \pm 0.2$ GPa),

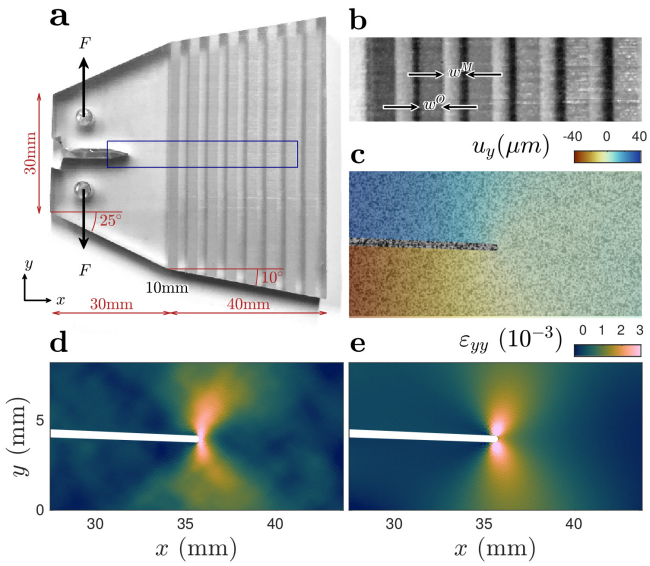

FIG. 1. (a) Model heterogeneous material made of multi-material 3D-printed polymers in a tapered double cantilever beam geometry with applied forces F. The displacement field $\boldsymbol{u} = (u_x, u_y)$ is measured in the area within the blue box by digital image correlation. (b) Closeup view shows two different materials in a periodic stripe geometry. The transparent material constitutes the matrix with width w^M and the opaque (darker) areas are obstacles of higher fracture energy $\Gamma^O/\Gamma^M \approx 1.3$ with width w^O. (c) Closeup of crack tip at $l \approx 35$mm and $v \approx 50$m/s. The crack interface is slightly visible running from left to center. A random speckle pattern is applied onto the surface, which is compared to its reference pre-cracked configuration to find $\boldsymbol{u}$. (d) Infinitesimal strain $\varepsilon_{yy} = \partial_y u_y$ found by differentiating $\boldsymbol{u}$. Approaching the crack tip, ε_{yy} diverges. (e) ε_{yy} assuming the Williams eigenfunctions as basis for $\boldsymbol{u}$.

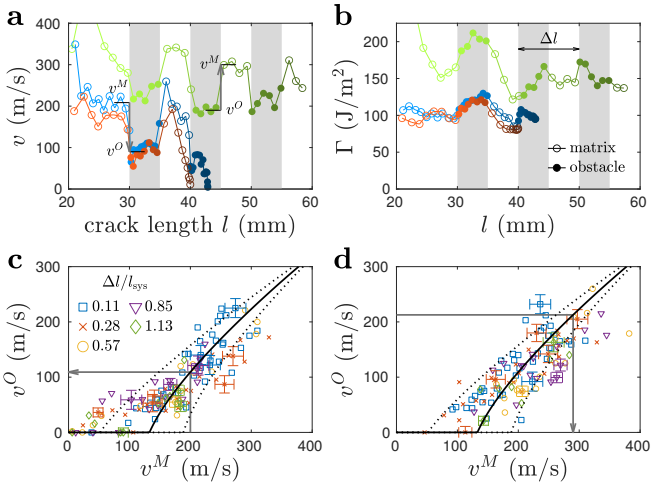

FIG. 2. (a,b) Experimental results for three specimens with $\Delta l/l_{\rm sys} = 0.57$. (a) v undergoes abrupt deceleration ($l = \{30, 40, 50\}$mm) and acceleration ($l = \{35, 45, 55\}$mm) when the crack front is trapped and untrapped, respectively, at the interface. (b) Discontinuities in Γ occur at trapping and untrapping with higher values within the obstacle. (c) Trapping: speed prior to entering the obstacle v^M is plotted vs. speed immediately after v^O. When the approaching velocity $v^M < v_c \approx 130$ m/s the front arrests. (d) Untrapping: speed after exiting the obstacle v^M is plotted vs. speed immediately before exiting v^O. (c,d) Solid black line is the theoretical model (2) with $\pm 10\%$ variation in Γ (dotted lines).

which is tougher and more compliant. We prescribe a constant crack mouth displacement rate $\dot{\delta} \approx 25$mm/s. Hence, the elastic energy in the system is gradually increased, until a planar crack initiates from a pre-existing notch. The elastic energy release rate at initiation is proportional to the bluntness of the notch, which we can tune to explore a range of initial crack speeds from moderate up to 350 m/s $\approx 0.4 c_{\rm R}$, where $c_{\rm R} \approx 800$m/s is the Rayleigh wave speed. The crack propagates then dynamically through a series of periodic obstacles (see FIG. 1b). During crack propagation no additional energy is added to the system (δ is constant) and the tapered geometry causes exponentially decaying released elastic energy $G^{\rm S} \sim \delta^2 e^{-l/l_{\rm sys}}$, where $l_{\rm sys} \approx 17.5$ mm is a structural length scale directly related to the sample size [28]. Thus, the crack speed gradually decreases on average. All properties are constant through the sample thickness and the overall behavior is quasi-2D. We analyze the crack dynamics by measuring the near-tip displacement field $\boldsymbol{u}$ using Digital Image Correlation. We apply a random speckle pattern (see FIG. 1c) onto the surface of the specimen using aerosol paint. The temporal evolution of the speckle is tracked using high speed photography at 250,000 fps. The auto-correlation length of the pattern corresponds to 4-6 pixels, where the pixel size is $\approx 45\mu$m. $\boldsymbol{u}$ (see color in FIG. 1c) is found by minimizing the difference between the pattern at a given time t mapped back to its pre-crack configuration [29]. The resulting infinitesimal strain field ε_{yy} is depicted in FIG. 1d. An alternative approach (see FIG. 1e) is the Integrated Digital Image Correlation (IDIC) [28, 30], which assumes the analytical solution for a singular crack in an infinite elastic medium – the Williams eigenfunctions expansion [31] – as basis for $\boldsymbol{u}$ [29]. The first term of the series has singular strains at the crack tip $\varepsilon_{ij} \sim 1/\sqrt{r}$, where r is the distance from the tip and its amplitude is related to the stress intensity factor K. Note that for both methods the amplitude of ε is similar. IDIC has the advantages of precisely determining the crack tip position l and directly computing K, from which, one can find the dynamic energy release rate $G = \frac{K^2}{E} A(v)$ that provides a measure of the fracture energy Γ at the crack tip [17, 29, 32]. The effects of elastic heterogeneity are minor in our setup, but give rise to an interaction between the size of the K-dominant region ($r \lesssim 5$mm) with the size of the heterogeneity and are discussed in [29].

Typical experiments are illustrated in FIG. 2a&b. The crack first propagates through the matrix material with

propagation speed v being maximum immediately after initiation, then v gradually decreases as crack length increases. v undergoes abrupt deceleration (acceleration) as the front enters (leaves) an obstacle. Simultaneously, Γ also abruptly increases (decreases). However, the relative jumps of the dissipation rate are significantly smaller than the ones observed on crack speed. We calculate the speed in the obstacle v^O and matrix v^M by selecting the mean speed over 12μs before and after the obstacle boundaries. All speed jumps at material discontinuities were studied for a collection of 30 experiments with different period $\Delta l = w^O + w^M$ and constant obstacle density $\beta = \frac{w^O}{w^O+w^M} = 1/2$. Jumps as the crack enters (trapping) and leaves (untrapping) an obstacle are shown in FIG. 2c&d, respectively. Results show that the crack dynamics at the matrix/obstacle interface is independent of obstacle width and is symmetric with respect to the direction of propagation, *i.e.*, the jumps are the same for trapping and untrapping. This implies that the crack dynamics only depends on local fracture properties.

In order to understand the jumps and their effect on effective material properties, we analyze the fracture propagation with a crack-tip energy balance. In our experiments, failure mechanisms occur at time scales 4 orders of magnitude smaller than the viscous relaxation time typical of the polymers used in this study [29] so that an elastic response of the sample can be safely assumed. Moreover, the failure mechanisms are too fast for a craze to develop [33], making the fracture process essentially brittle. Thus, we develop a theoretical model based on LEFM to interpret the experimental observations.

As the crack advances, elastic energy G^{S} is released from the specimen and is in part dissipated as fracture energy Γ to create new surfaces and in part radiated away as elastic waves. Analyzing the near-tip fields of a steady-state dynamic crack, Freund [17] showed that the energy release rate of a dynamic crack $G(l, v)$ is related to the energy release rate for a corresponding static crack $G^{\mathrm{S}}(l)$ by $g(v)$, a universal function of v. The crack-tip energy balance provides the equation of motion for a crack [29]

$$\Gamma(v) = G^{\mathrm{S}}(l)g(v) \approx G^{\mathrm{S}}(l)(1 - v/c_{\mathrm{R}}), \qquad (1)$$

which implies that within the framework of LEFM, a sub-Rayleigh crack in an infinite medium has no inertia and v adjusts instantaneously to fluctuations in Γ or G^{S} [29]. Note that for rate-dependent materials, the fracture energy $\Gamma(v)$ is not constant.

We analyze the rate-dependence of the matrix and obstacle material by independently plotting Γ vs. v (see averaged data as dashed line in FIG. 3 or full data in FIG. S3 of [29]). We observe that our measurements are in good agreement with a model [25] (solid line in FIG. 3) that considers the actual dissipative mechanism taking place within the process zone. Within the matrix or obstacle material, the fracture energy follows this kinetic

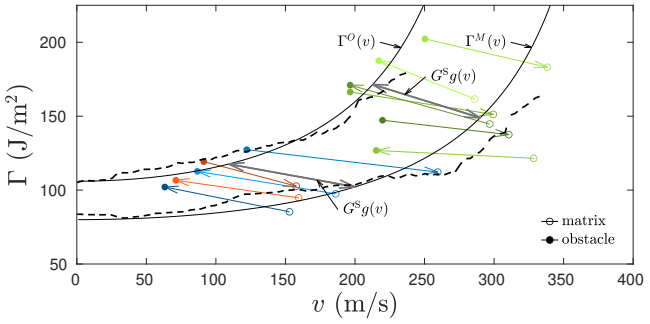

FIG. 3. Experimental results for the same specimens shown in FIG. 2a&b – with same color-code. Data points represent crack speed and fracture energy at the moment of transition of material property. $\Gamma(v)$ is separated in two distinct clusters corresponding to the matrix and obstacle material. Black dashed lines are the average fracture energy measurements based on 30 heterogeneous and 10 homogeneous samples [29]. Solid black lines are the rate-dependent fracture energy law [25] for the obstacle $\Gamma^O(v)$ and matrix $\Gamma^M(v)$ materials. The transition from one branch to the other is described by $G^{\mathrm{S}}(l)g(v)$ – the equation of the gray arrows (1).

law. At the material boundaries, however, the rupture needs to jump from one kinetic law to the other. The jump amplitude is governed by the equation of motion (1). The jump trajectory in the Γ-v space corresponds to the right-hand side of (1), which, since $G^{\mathrm{S}}(l)$ is constant across the boundary, corresponds to a diagonal line $G^{\mathrm{S}}g(v)$ (arrows in FIG. 3).

Thus, at a discontinuity in material property the equation of motion of a crack becomes

$$G^{\mathrm{S}} = \Gamma^M(v^M)/g(v^M) = \Gamma^O(v^O)/g(v^O)\ , \qquad (2)$$

which captures the experimentally observed velocity discontinuity at trapping and untrapping with no fitting parameter (see FIG. 2c&d). Eq. (2) cannot be solved explicitly. However, assuming a *linear* rate-dependent fracture energy $\Gamma(v) \approx \Gamma_0 + \gamma v$, for the purpose of discussion, the velocity jump becomes

$$v^M - v^O \approx \Delta\Gamma_0 \frac{1 - v^M/c_{\mathrm{R}}}{\gamma + \Gamma_0^M/c_{\mathrm{R}}}\ , \qquad (3)$$

where $\Delta\Gamma_0 = \Gamma_0^O - \Gamma_0^M$ is the jump in fracture energy. This simple result highlights that (i) the jump amplitude is the same for trapping and untrapping (FIG. 2c&d) and (ii) during trapping the velocity right after the interface is zero if v^M is smaller than a critical incident velocity v_{c} below which the obstacle causes crack arrest

$$v_{\mathrm{c}} \approx \Delta\Gamma_0 / \left(\gamma + \Gamma_0^O/c_{\mathrm{R}}\right)\ . \qquad (4)$$

All these features are discernible from our experimental data and are captured fairly well by the model. Eq. (3) as well as a parameter study of (2) (see FIG. S3

in [29]) reveal that the speed jump and v_c are proportional to the toughness discontinuity $\Delta\Gamma_0$. The latter is particularly noisy because of variations of fracture properties of both matrix and obstacle material, *i.e.*, $\mathrm{Var}[\Delta\Gamma_0] = \mathrm{Var}[\Gamma_0^M] + \mathrm{Var}[\Gamma_0^O]$, assuming Γ_0^O and Γ_0^M are uncorrelated. In the limit of small rate-dependency $\gamma \ll \Gamma_0/c_R$, inertia controls the speed jumps, that are then given by $v^M - v^O \approx (\Delta\Gamma_0/\Gamma_0^M)(c_R - v^M)$ and the corresponding condition for crack arrest becomes $v < v_c \approx (\Delta\Gamma_0/\Gamma_0^O)c_R$. Conversely, in the limit of large rate-dependency $\gamma \gg \Gamma_0/c_R$ and quasi-static propagation $v \ll c_R$, inertia can be neglected and the speed jumps become constant $v^M - v^O \approx \Delta\Gamma_0/\gamma \equiv v_c$.

How does such a trapping/untrapping dynamics impact the effective fracture properties $\bar{\Gamma}$ of heterogeneous materials? We compute the homogenized fracture energy $\bar{\Gamma}$ by integrating over an interval Δl of uninterrupted crack propagation starting at l_i, the beginning of each matrix/obstacle period,

$$\bar{\Gamma}(\bar{v}) = \frac{1}{\Delta l}\int_{l_i}^{l_i+\Delta l} \Gamma\left(v(\tilde{l})\right) \mathrm{d}\tilde{l}\ . \tag{5}$$

As Γ in each phase depends on crack speed, $\bar{\Gamma}$ depends on it too. Thus, we report $\bar{\Gamma}$ as a function of the apparent crack velocity $\bar{v} = \Delta l / \int_{l_i}^{l_i+\Delta l} v^{-1}\mathrm{d}l$.

First, we assume $\Delta l \ll l_{\mathrm{sys}}$, *i.e.*, a clear separation between the micro-structural scale and the specimen scale. Hence, it is possible to define *intrinsic* homogenized fracture properties, decoupled from the specimen size and the details of applied boundary conditions. Under this assumption, G^{S} remains constant during the entire crack propagation. Thus, v and Γ are constant within each material phase (insets in FIG. 4a), which allows us to calculate the dissipation rate from (5)

$$\lim_{\Delta l/l_{\mathrm{sys}}\to 0} \bar{\Gamma} = \beta\Gamma^O(v^O) + (1-\beta)\Gamma^M(v^M) \tag{6}$$

and the apparent crack speed

$$\lim_{\Delta l/l_{\mathrm{sys}}\to 0} \bar{v} = \left(\beta/v^O + (1-\beta)/v^M\right)^{-1}, \tag{7}$$

with $\beta = 1/2$. Note that (7) is a weighted harmonic mean, which is dominated by its lower argument, v^O, so $\bar{v}$ is effectively lower than the arithmetic mean ($\langle v\rangle = \beta v^O + (1-\beta)v^M$). As a result, the apparent kinetic law $\bar{\Gamma}(\bar{v})$ is shifted "horizontally" towards lower speeds in comparison to $\bar{\Gamma}(\langle v\rangle)$. This leads, in practice, to a resistance to failure $\bar{\Gamma}$ *larger* than the toughness spatial average $\langle\Gamma\rangle = \beta\Gamma^O(\bar{v}) + (1-\beta)\Gamma^M(\bar{v})$, but lower than the obstacle toughness Γ^O predicted by rate-independent theory (see FIG. 4).

However, when comparing the infinite system size prediction (6) and (7) to our experimental measurements we observe higher effective toughness (see FIG. 4b). The interplay between the size of the heterogeneity Δl and the

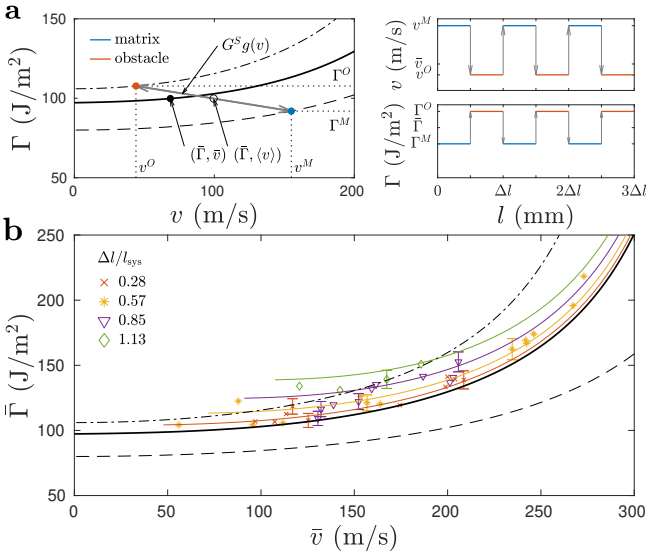

FIG. 4. Homogenization of fracture energy $\bar{\Gamma}$ vs. average velocity, $\bar{v}$. (a) $\bar{\Gamma}$ assuming the scale separation condition $\Delta l \ll l_{\mathrm{sys}}$. Blue and red dots represent the state of the crack within the two materials, which are related by (2) depicted as a gray arrow. The black dot is the corresponding homogenized state $(\bar{\Gamma}, \bar{v})$ computed using (6) and (7). By varying G^{S} one can derive the entire homogenized fracture energy law $\bar{\Gamma}(\bar{v})$ (black solid line in a&b). (b) $\bar{\Gamma}(\bar{v})$, measured experimentally using (5), is depicted as colored circles for a range of $\Delta l \approx l_{\mathrm{sys}}$. Colored solid lines are the theoretical solution for $\Delta l \approx l_{\mathrm{sys}}$ derived using (5), (1) [29] (theory and experiment colors correspond). (a,b) Dash-dotted line and dashed line are $\Gamma^O(v)$ and $\Gamma^M(v)$ from FIG 3.

structural length scale l_{sys} makes homogenization of fracture properties particularly challenging. The emerging effective toughness depends on the ratio $\Delta l/l_{\mathrm{sys}}$, and (6) and (7) only represent a lower bound of $\bar{\Gamma}(\bar{v})$. The larger $\Delta l/l_{\mathrm{sys}}$, the higher $\bar{\Gamma}(\bar{v})$, which can even exceed $\Gamma^O(\bar{v})$ of the obstacle material. This additional toughening, related to the structural problem with $\Delta l \approx l_{\mathrm{sys}}$, is quantitatively captured by the theoretical solutions for $\bar{\Gamma}(\bar{v})$, which we derive from (5) and (1), assuming $G^{\mathrm{S}} \sim e^{-l/l_{\mathrm{sys}}}$. Note that as we approach $\Delta l \ll l_{\mathrm{sys}}$, the experimental toughness converges towards the theoretical one; and for $\Delta l \gg l_{\mathrm{sys}}$ the rupture arrests before reaching Δl required for homogenization of fracture properties.

How do these observations translate to macroscopic measurements? While measurements from total elastic energy input (see FIG. S5 in [29]) present increased toughness compared to the matrix material, they do not exceed the obstacle material. This is because the additional toughening observed at the small scale is a "horizontal shift" of the kinetic law. However, we observe that the macroscopic fracture energy is independent of Δl and corresponds to the average of matrix and obstacle material, which validates (6). Furthermore, crack arrest, as described by (4), may play an important role in further

increasing the macroscopic toughness. Even very thin obstacles may cause the crack to arrest, which raises interesting questions of practical importance for material design. How to design flaw insensitive materials, whose resistance to crack propagation – or ability to prevent a crack to grow indefinitely – is directly proportional to the obstacle toughness but independent of its size? What are the strategies to translate this local toughening to the macro-scale and improve the mechanical integrity of structures through the use of damage-tolerant composites?

In summary, our study shows that the classical LEFM equation of motion of cracks quantitatively predicts crack dynamics at toughness discontinuities. The crack arrests if it is slower than a threshold speed that is primarily dependent on the toughness contrast and independent of the characteristic size of the microstructure (*i.e.*, obstacle thickness), *i.e.*, (4). When the crack penetrates the tougher/weaker obstacle, it reacts by instantaneously adapting its speed, which is mediated by the rate-dependent fracture energy combined with inertia, *i.e.*, (3). Finally, the heterogeneous material presents an increased effective (homogenized) toughness because of high fluctuations in crack speed between obstacles and matrix, and the rate-dependent nature of the fracture energy. Direct experimental validation of (3) and (4) is challenging due to limited temporal resolution and fluctuations in Γ, but increased toughness contrast and focus on a single interface could provide a path to overcome these limitations.

The authors thank Dr. Thiago Melo Grabois and Dr. Julien Scheibert for useful discussions.

* dkammer@ethz.ch

[1] R. O. Ritchie, Nature Materials **10**, 817 (2011).

[2] Jackson A. P., Vincent Julian F. V., Turner R. M., and Alexander Robert Mcneill, Proceedings of the Royal Society of London. Series B. Biological Sciences **234**, 415 (1988).

[3] B. Florijn, C. Coulais, and M. van Hecke, Physical Review Letters **113**, 175503 (2014).

[4] M. K. Blees, A. W. Barnard, P. A. Rose, S. P. Roberts, K. L. McGill, P. Y. Huang, A. R. Ruyack, J. W. Kevek, B. Kobrin, D. A. Muller, and P. L. McEuen, Nature **524**, 204 (2015).

[5] K. Bertoldi, P. M. Reis, S. Willshaw, and T. Mullin, Advanced Materials **22**, 361 (2010).

[6] J. L. Silverberg, A. A. Evans, L. McLeod, R. C. Hayward, T. Hull, C. D. Santangelo, and I. Cohen, Science **345**, 647 (2014).

[7] E. Siéfert, E. Reyssat, J. Bico, and B. Roman, Nature Materials **18**, 24 (2019).

[8] Z. Yin, F. Hannard, and F. Barthelat, Science **364**, 1260 (2019), publisher: American Association for the Advancement of Science Section: Report.

[9] H. Gao and J. R. Rice, Journal of Applied Mechanics **56**, 828 (1989).

[10] S. Roux, D. Vandembroucq, and F. Hild, European Journal of Mechanics - A/Solids General and plenary lectures from the 5th EUROMECH Solid Mechanics Conference, **22**, 743 (2003).

[11] L. Ponson and N. Pindra, Physical Review E **95**, 053004 (2017).

[12] M. Lebihain, J.-B. Leblond, and L. Ponson, Journal of the Mechanics and Physics of Solids **137**, 103876 (2020).

[13] M. Z. Hossain, C. J. Hsueh, B. Bourdin, and K. Bhattacharya, Journal of the Mechanics and Physics of Solids **71**, 15 (2014).

[14] N. Wang and S. Xia, Journal of the Mechanics and Physics of Solids **98**, 87 (2017).

[15] A. A. Griffith and G. I. Taylor, Philosophical Transactions of the Royal Society of London. Series A, Containing Papers of a Mathematical or Physical Character **221**, 163 (1921), publisher: Royal Society.

[16] J. R. Rice, Journal of the Mechanics and Physics of Solids **26**, 61 (1978).

[17] L. B. Freund, *Dynamic Fracture Mechanics* (Cambridge University Press, Cambridge, 1990).

[18] L. Ponson, Physical Review Letters **103**, 055501 (2009).

[19] B. K. Atkinson, Journal of Geophysical Research: Solid Earth **89**, 4077 (1984).

[20] E. Sharon and J. Fineberg, Nature **397**, 333 (1999).

[21] A. Livne, E. Bouchbinder, I. Svetlizky, and J. Fineberg, Science **327**, 1359 (2010).

[22] B. T. Aagaard and T. H. Heaton, Bulletin of the Seismological Society of America **94**, 2064 (2004).

[23] T. Goldman, A. Livne, and J. Fineberg, Physical Review Letters **104**, 114301 (2010).

[24] T. Goldman, R. Harpaz, E. Bouchbinder, and J. Fineberg, Physical Review Letters **108**, 104303 (2012).

[25] J. Scheibert, C. Guerra, F. Célarié, D. Dalmas, and D. Bonamy, Physical Review Letters **104**, 10.1103/PhysRevLett.104.045501 (2010).

[26] A. Vasudevan, T. M. Grabois, G. C. Cordeiro, S. Morel, R. D. T. Filho, and L. Ponson, arXiv:2101.04380 [cond-mat] (2021), arXiv: 2101.04380.

[27] A. J. Rosakis and A. T. Zehnder, International Journal of Fracture **27**, 169 (1985), place: Dordrecht Publisher: Kluwer Academic Publishers.

[28] T. M. Grabois, J. Neggers, L. Ponson, F. Hild, and R. D. Toledo Filho, Engineering Fracture Mechanics **191**, 311 (2018).

[29] See supplemental material at [url will be inserted by publisher] for dynamic crack propagation theory, fracture energy measurements, equation of motion for a crack and integrated digital image correlation method based on the williams eigenfunctions. the equation of motion is applied to the trapping and untrapping and to the homogenization of fracture energy problems.

[30] S. Roux and F. Hild, International Journal of Fracture **140**, 141 (2006).

[31] M. L. Williams, Journal of Applied Mechanics **24**, 109 (1956).

[32] I. Svetlizky and J. Fineberg, Nature **509**, 205 (2014).

[33] K. Ravi-Chandar and M. Balzano, Engineering Fracture Mechanics **30**, 713 (1988).